

Supplementary Materials for
Microtubule-binding core of the tau protein

Nadia El Mammeri *et al.*

Corresponding author: Mei Hong, meihong@mit.edu

Sci. Adv. **8**, eabo4459 (2022)
DOI: 10.1126/sciadv.abo4459

This PDF file includes:

Tables S1 to S4
Figs. S1 to S11
References

Table S1. Chemical shifts (^{13}C ppm / ^1H ppm) of highly mobile residues in the INEPT spectra of microtubule-bound P2R tau (1 : 1). Random coil chemical shift values (56) are shown in brackets below the measured chemical shifts for tau.

Residues	C α /H α	C β /H β	C γ 1/H γ 1	C γ 2/H γ 2	C δ 1/H δ 1	C δ 2/H δ 2	C ϵ 1/H ϵ 1
Thr		67.8 / 4.2 (67.8 / 4.2)		20.0 / 1.2			
Thr(Pro)	61.6 / 4.7						
Ser		62.1 / 3.9 (61.9 / 3.9)					
Ser(Pro)		61.0 / 3.9 (61.9 / 3.9)					
Ala		17.7 / 1.4 (17.0 / 1.4)					
Ala(Pro)	51.6 / 4.7 (50.7 / 4.5)	16.4 / 1.4 (17.0 / 1.4)					
Pro			25.4 / 2.1		49.1 / 3.7		
Gly	43.8 / 3.9 (43.3 / 4.0)						
Arg					41.7 / 3.1		
Lys			23.2 / 1.5				40.3 / 3.0
Asn		37.5 / 2.8 (36.2 / 2.8)					
Glu			34.7 / 2.2				
Gln			32.1 / 2.4				
Leu		40.1 / 1.7 (39.9 / 1.6)			23.4 / 0.9 (22.7 / 1.6)	21.5 / 0.9 (22.1 / 0.7)	
Val			19.2 / 0.9				
Ile		36.6 / 1.8 (36.3 / 1.8)	25.6 / 1.2	16.0 / 0.8	11.5 / 0.8		
Met							15.3 / 2.1
His						118.4 / 7.1	135.6 / 8.2

Table S2. 2D INEPT intensity analysis of MT-bound P2R tau (1 : 1) and number of amino acid residues in different domains of P2R tau. The first two rows show the integrated intensities relative to the signals of A(P) C β and Met C ϵ . The last column gives the RMSD values between the residue numbers in each domain and the INEPT-detected number of flexible residues based on the Ala C β signal. The P2-R1 segment (residues 198-253) shows low RMSD, suggesting that this domain best encapsulates the most mobile residues in MT-bound P2R tau. The T(P) signal partially overlaps with a weak Pro C α peak, thus its integrated intensity represents an upper bound.

Tau domains	A CB	A(P) CB	G CA	I CB	L CB	S CB	S(P) CB	K CG	R CD	Q CG	E CG	T CB	T(P) CB	M CE	RMSD
INEPT: A(P)C β	2.0	1.0	2.2	1.4	0.8	6.2	3.3	7.1	2.5	2.5	3.5	4.0	3.1	0.9	
INEPT: MC ϵ	2.1	1.1	2.3	1.5	0.9	6.6	3.5	7.5	2.7	2.6	3.7	4.2	3.3	1.0	
P2(198-243)	2	0	4	0	2	7	3	4	5	0	1	5	4	0	1.8
R1(244-274)	0	1	4	1	2	2	0	5	0	2	1	2	0	1	2.2
R2(275-305)	0	0	4	3	2	4	0	5	0	2	0	0	0	0	2.4
R3(306-336)	0	0	5	2	2	3	0	4	0	2	0	1	0	0	2.5
R4(337-368)	0	0	4	2	2	3	0	4	1	1	2	1	0	0	2.2
R'(369-399)	3	0	1	1	1	0	1	6	1	0	3	3	0	0	2.2
P2-R1(198-253)	2	1	4	0	3	7	3	5	5	1	1	6	0	1	1.7

Table S3. ^{13}C and ^{15}N chemical shifts (ppm) of immobilized residues in microtubule-bound P2R tau measured from dipolar NMR spectra.

Residues	$\text{C}\alpha$	$\text{C}\beta$	C'	N	$\text{C}\gamma/\gamma1$	$\text{C}\gamma2$	$\text{C}\delta/\delta1$	$\text{C}\delta2$	$\text{C}\epsilon/\epsilon1$	$\text{C}\epsilon2/\zeta$	$\text{N}\delta$
<i>Sequentially assigned residues</i>											
I354	59.1	37.3	173.7		16.0		22.6		11.8		
G355	45.2		174.7	111.6							
S356	56.4	61.6	172.3	114.5							
L357	53.6	40.1	173.2	123.5	27.1		22.7				
D358	51.8	38.4	176.5	118.9	178.2						
H362	55.9	28.2	172.3	122.3							
V363	56.2	31.7	171.2	129.3	18.3						
P364	60.6	30.5	175.6	137.5	25.7		48.7				
G365	41.3		171.9	112.4							
G366	42.5		173.4	104.1							
G367	44.3		173.1	105.8							
A382	51.0	17.0	176.3	124.9							
K383	54.3	33.8		121.6	23.9		27.5		39.8		
T386	59.3	66.9	172.8		19.9						
D387	52.2	39.05	176.7	123.9							
H388	57.8	25.6	173.2	118.4							
G389	43.8		173.1	105.1							
S396	54.6	61.1	170.8	123.4							
P397	60.3			135.2			48.3				
Thr1		66.5			20.0						
Thr2	62.3	69.0			19.4						
<i>Type-assigned residues</i>											
Asn/Asp1	48.9	37.1	174.9	117.9							
Asn/Asp2	50.8	37.0	175.7	122.1							
Asn/Asp3	51.3	37.3		123.4							
Asn/Asp4	50.4	37.2	127.3								
Ile1					25.2	15.5	10.7				
Ile2	58.8	36.5	175.2			15.3					
Val1	61.6	29.9		121.3	19.2						
Val2	59.9	30.7		121.2	19.0						
Val3	56.1	31.8	172.5		18.5						
Val4	58.1		173.7		19.5						
Val5		30.0			20.4						
Gln/Glu1	53.5	30.8		126.1	27.8		184.6				
Phe/Tyr1	55.5	38.2		121.9							
Ala1	48.1		17.2	117.2							
Ala2	51.5	19.6		128.5							
Ala3	52.4	19.8									
Leu1	52.2				23.1	24.6					

Table S4. Solid-state NMR experimental parameters of microtubule-bound tau. All experiments were recorded on an 18.8 T spectrometer (800 MHz ^1H frequency). Reported temperatures are estimated sample temperatures based on the water ^1H chemical shift.

Experiment	NMR Parameters	Samples	Expt. Time
2D CC with 23-80 ms CORD mixing	$T_{\text{sample}} = 278 \text{ K}$; $\nu_{\text{MAS}} = 10.5 \text{ kHz}$, $ns = 64$, $\tau_{\text{rd}} = 1.7 \text{ s}$, $t_{1,\text{max}} = 8.7 \text{ ms}$; $t_{1,\text{inc}} = 24.8 \mu\text{s}$; $\tau_{\text{dwell}} = 6 \mu\text{s}$; $\tau_{\text{acq}} = 15.4 \text{ ms}$; $\tau_{\text{HC}} = 70\text{-}800 \mu\text{s}$; $\tau_{\text{CORD}} = 23\text{-}80 \text{ ms}$; $\nu_{1\text{Hacq}} = 71 \text{ kHz}$ TPPM	MT : P2R tau (1 : 1) MT : P2R tau (1 : 0.5) Tub : P2R tau (1 : 2)	110 hr 130 hr 65 hr
2D NCA SPECCP	$T_{\text{sample}} = 278 \text{ K}$; $\nu_{\text{MAS}} = 10.5 \text{ kHz}$, $ns = 256$, $\tau_{\text{rd}} = 1.7 \text{ s}$, $t_{1,\text{max}} = 9.5 \text{ ms}$; $t_{1,\text{inc}} = 95.2 \mu\text{s}$; $\tau_{\text{dwell}} = 6 \mu\text{s}$; $\tau_{\text{acq}} = 15.4 \text{ ms}$; $\tau_{\text{HN}} = 1 \text{ ms}$; $\tau_{\text{NC}} = 5.5 \text{ ms}$; $\nu_{15\text{NspecificCP}} = 26.3 \text{ kHz}$ ramp 90-100%; $\nu_{13\text{CspecificCP}} = 15.8 \text{ kHz}$; $\nu_{1\text{HspecificCP}} = 71 \text{ kHz}$ CW; $\nu_{1\text{Hacq}} = 71 \text{ kHz}$ TPPM	MT : P2R tau (1 : 1) MT : P2R tau (1 : 0.5) MT : 0N4R tau (1 : 1) Tub : P2R tau (1 : 2)	50 hr 80 hr 46 hr 75 hr
2D NCO SPECCP	$T_{\text{sample}} = 278 \text{ K}$; $\nu_{\text{MAS}} = 14 \text{ kHz}$, $ns = 256/352$, $\tau_{\text{rd}} = 1.7 \text{ s}$, $t_{1,\text{max}} = 9.3 \text{ ms}$; $t_{1,\text{inc}} = 142.9 \mu\text{s}$; $\tau_{\text{dwell}} = 6 \mu\text{s}$; $\tau_{\text{acq}} = 15.4 \text{ ms}$; $\tau_{\text{HN}} = 3 \text{ ms}$; $\tau_{\text{NC}} = 5 \text{ ms}$; $\nu_{15\text{NspecificCP}} = 25.2 \text{ kHz}$ ramp 90-100%; $\nu_{13\text{CspecificCP}} = 39.2 \text{ kHz}$; $\nu_{1\text{HspecificCP}} = 71 \text{ kHz}$ CW; $\nu_{1\text{Hacq}} = 71 \text{ kHz}$ TPPM	MT : P2R tau (1 : 1)	38 hr
2D N(CO)CA SPECCP-BSHCP	$T_{\text{sample}} = 278 \text{ K}$; $\nu_{\text{MAS}} = 14 \text{ kHz}$, $ns = 512$, $\tau_{\text{rd}} = 1.7 \text{ s}$, $t_{1,\text{max}} = 6.4 \text{ ms}$; $t_{1,\text{inc}} = 142.9 \mu\text{s}$; $\tau_{\text{dwell}} = 6 \mu\text{s}$; $\tau_{\text{acq}} = 15.4 \text{ ms}$; $\tau_{\text{HN}} = 3 \text{ ms}$; $\tau_{\text{NC}} = 5 \text{ ms}$; $\tau_{\text{CC}} = 4.5 \text{ ms}$; $\nu_{15\text{NspecificCP}} = 25.2 \text{ kHz}$ 90-100% ramp; $\nu_{13\text{CspecificCP}} = 39.2 \text{ kHz}$; $\nu_{1\text{HspecificCP}} = 71 \text{ kHz}$ CW; $\nu_{1\text{Hacq}} = 83 \text{ kHz}$ TPPM; $\nu_{1\text{HBShCP}} = 90 \text{ kHz}$ CW	MT : 0N4R tau (1 : 1)	88 hr
2D ^1H - ^{13}C INEPT	$T_{\text{sample}} = 278 \text{ K}$; $\nu_{\text{MAS}} = 10.5 \text{ kHz}$, $ns = 112$, $\tau_{\text{rd}} = 2 \text{ s}$, $t_{1,\text{max}} = 15.9 \text{ ms}$; $t_{1,\text{inc}} = 124.8 \mu\text{s}$; $\tau_{\text{dwell}} = 6 \mu\text{s}$; $\tau_{\text{acq}} = 24.6 \text{ ms}$; $\nu_{1\text{Hacq}} = 71 \text{ kHz}$ TPPM	MT : P2R tau (1 : 1) MT : P2R tau (1 : 0.5)	17 hr 17 hr
2D N(CA)CB SPECCP-DREAM	$T_{\text{sample}} = 278 \text{ K}$; $\nu_{\text{MAS}} = 14 \text{ kHz}$, $ns = 480$, $\tau_{\text{rd}} = 1.7 \text{ s}$, $t_{1,\text{max}} = 6.4 \text{ ms}$; $t_{1,\text{inc}} = 142.9 \mu\text{s}$; $\tau_{\text{dwell}} = 6 \mu\text{s}$; $\tau_{\text{acq}} = 15.4 \text{ ms}$; $\tau_{\text{HN}} = 3 \text{ ms}$; $\tau_{\text{NC}} = 5.5 \text{ ms}$; $\tau_{\text{CC}} = 2 \text{ ms}$; $\nu_{15\text{NspecificCP}} = 26.3\text{kHz}$ 90-100% ramp; $\nu_{13\text{CspecificCP}} = 15.8 \text{ kHz}$; $\nu_{1\text{HspecificCP}} = 83 \text{ kHz}$ CW; $\nu_{1\text{Hacq}} = 83 \text{ kHz}$ TPPM; $\nu_{1\text{HDREAM}} = 83 \text{ kHz}$ CW	MT : 0N4R tau (1 : 1)	84 hr
1D ^{13}C DP	$T_{\text{sample}} = 278 \text{ K}$; $\nu_{\text{MAS}} = 10.5 \text{ kHz}$, $ns = 4096$, $\tau_{\text{rd}} = 3 \text{ s}$, $\tau_{\text{dwell}} = 6 \mu\text{s}$; $\tau_{\text{acq}} = 15.4 \text{ ms}$; $\nu_{1\text{Hacq}} = 83 \text{ kHz}$ TPPM	MT : P2R tau (1 : 1) MT : P2R tau (1 : 0.5) MT : 0N4R tau (1 : 1) MT only	3.5 hr 3.5 hr 3.5 hr 3.5 hr
1D ^{13}C CP	$T_{\text{sample}} = 278 \text{ K}$; $\nu_{\text{MAS}} = 10.5 \text{ kHz}$, $ns = 4096$, $\tau_{\text{rd}} = 1.7 \text{ s}$, $\tau_{\text{dwell}} = 6 \mu\text{s}$; $\tau_{\text{acq}} = 15.3 \text{ ms}$; $\tau_{\text{HC}} = 70/800 \mu\text{s}$; $\nu_{1\text{Hacq}} = 71 \text{ kHz}$ TPPM	MT : P2R tau (1 : 1) MT : P2R tau (1 : 0.5) MT : 0N4R tau (1 : 1) MT only	2 hr 2 hr 2 hr 2 hr
1D ^{13}C INEPT	$T_{\text{sample}} = 278 \text{ K}$; $\nu_{\text{MAS}} = 10.5 \text{ kHz}$; $ns = 4096$, $\tau_{\text{rd}} = 2 \text{ s}$; $\tau_{\text{dwell}} = 6 \mu\text{s}$; $\tau_{\text{acq}} = 24.6 \text{ ms}$; $\nu_{1\text{Hacq}} = 71 \text{ kHz}$ TPPM	MT : P2R tau (1 : 1) MT : P2R tau (1 : 0.5) MT : 0N4R tau (1 : 1) MT only	2.5 hr 2.5 hr 2.5 hr 2.5 hr
1D water-edited ^{13}C CP	$T_{\text{sample}} = 278 \text{ K}$; $\nu_{\text{MAS}} = 10.5 \text{ kHz}$, $ns = 1024$, $\tau_{\text{rd}} = 1.7 \text{ s}$; $\tau_{\text{dwell}} = 6 \mu\text{s}$; $\tau_{\text{acq}} = 15.3 \text{ ms}$; $\tau_{1\text{Hsel}} = 950 \mu\text{s}$; $\tau_{\text{filter}} = 95 \mu\text{s} \times 10$; $\tau_{\text{SD}} = 0/4/16/36/100 \text{ ms}$; $\tau_{\text{HC}} = 70 \mu\text{s}$; $\nu_{1\text{Hacq}} = 71 \text{ kHz}$ TPPM	MT : P2R tau (1 : 1) MT : P2R tau (1 : 0.5) MT : 0N4R tau (1 : 1) MT only	2.5 hr 2.5 hr 2.5 hr 2.5 hr

Symbols: T_{sample} = sample temperature; ν_{MAS} = MAS frequency; ns = number of scans (transients) per free induction decay (FID); τ_{rd} = recycle delay between scans; $t_{1,\text{max}}$ = maximum t_1 (indirect dimension 1) evolution time; $t_{1,\text{inc}}$ = increment for t_1 (indirect dimension 1) evolution time; τ_{dwell} = dwell time during direct FID acquisition; τ_{acq} = maximum acquisition time during direct FID detection; τ_{XY} = cross polarization (CP, $^{\text{SPECIFIC}}$ CP, BSH-CP, or DREAM) contact time during CP from channel X to channel Y; $\nu_{\text{nuc-CP,XY}}$ = radiofrequency field strength for CP spin lock on *nuc* (*nuc* = ^1H , ^{13}C , ^{15}N) during CP from X to Y; $\nu_{1\text{H,acq}}$ = dipolar decoupling field strength during FID acquisition and indirect dimension evolution; $\nu_{\text{nuc-DCP}}$ = rf spin lock field strength on *nuc* during heteronuclear CP; $\nu_{1\text{H-DD,DCP}}$ = ^1H

dipolar decoupling field strength during heteronuclear CP; τ_{DREAM} = spin lock contact time during homonuclear coherence transfer with the DREAM condition.

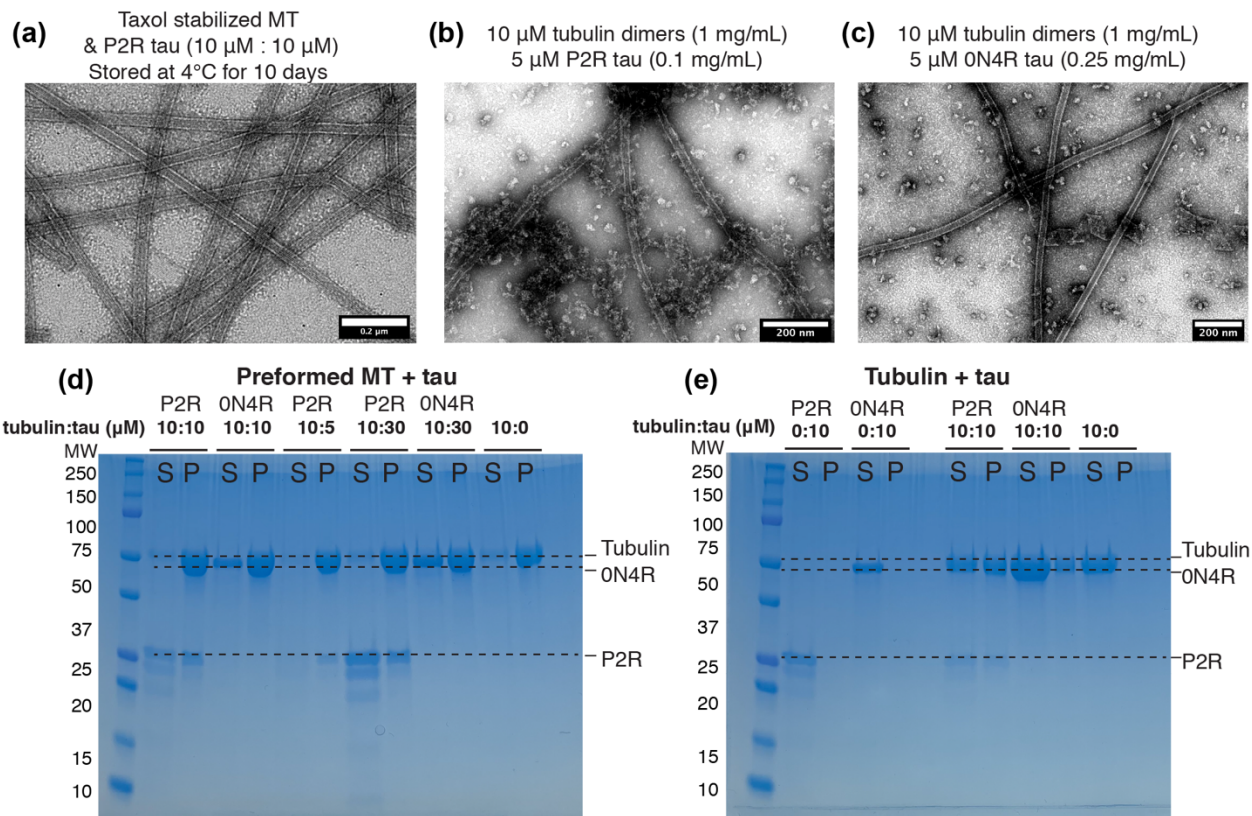


Figure S1. Characterization of P2R tau purity and tau-tubulin interactions. (a) TEM images of preformed microtubules with bound P2R tau (molar ratio 1 : 1). The sample was imaged after storage for 10 days at 4°C as a pellet, the same condition as samples used for solid-state NMR experiments. The microtubules remain intact, indicating that the solid-state NMR samples are stable over the duration of the experiments. (b) TEM images of microtubules co-assembled with P2R tau at a molar ratio of 1 : 0.5 for tubulin dimers : tau in the absence of taxol. (c) TEM images of microtubules co-assembled with ON4R tau at a molar ratio of 1 : 0.5 in the absence of taxol. (d) SDS-PAGE gel of the pellet (P) and supernatant (S) of preformed microtubules with varying concentrations of P2R tau after ultracentrifugation. Tubulin and P2R tau co-sediment into pellets, indicating that P2R tau binds microtubules. (e) SDS-PAGE gel of the pellet and supernatant of tubulin : tau mixtures prepared under similar conditions as those shown in (b) and (c) after ultracentrifugation.

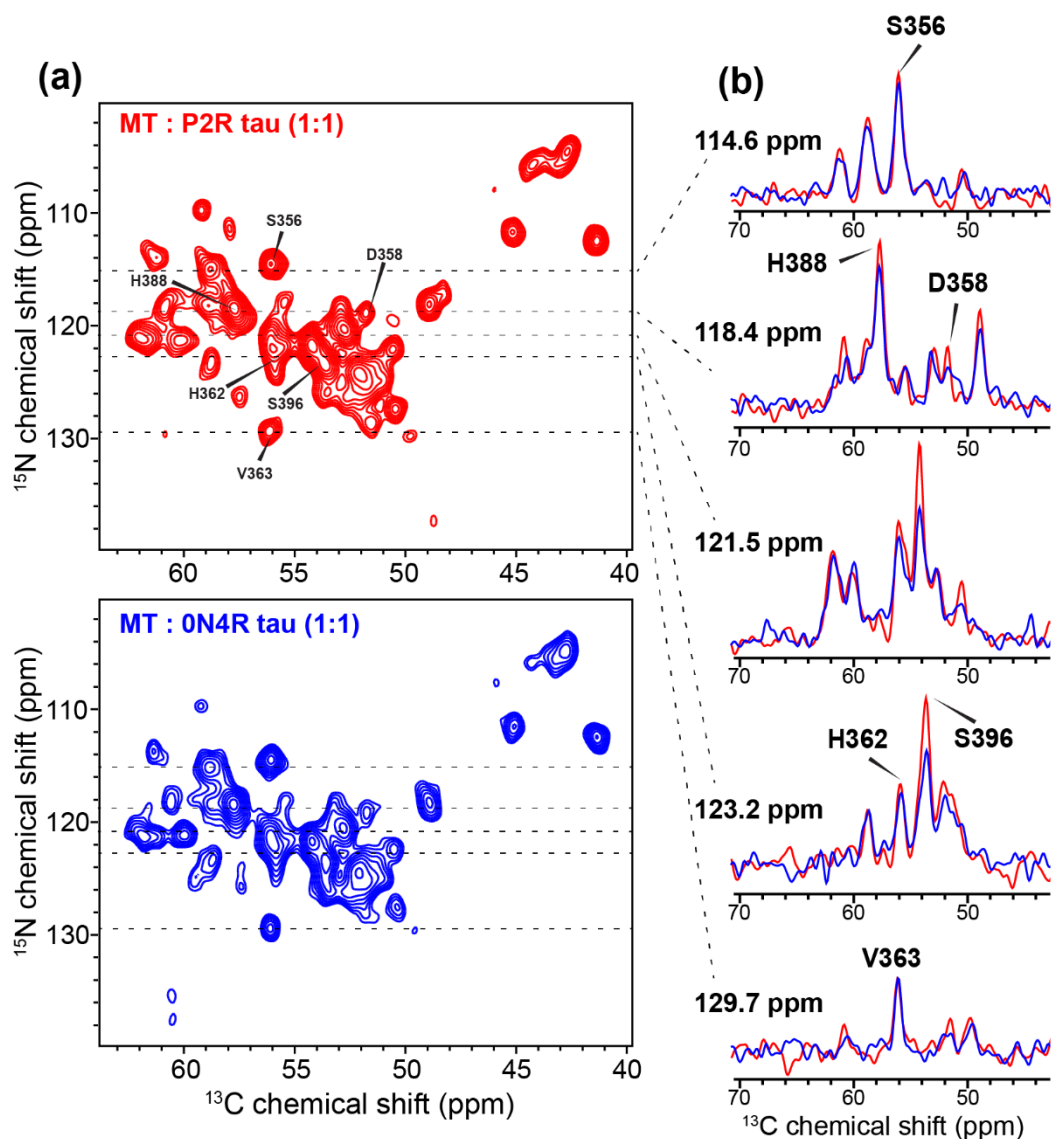


Figure S2. 1D ^{15}N cross sections of the 2D $\text{NC}\alpha$ spectra of microtubule-bound tau show good spectral sensitivity. (a) 2D spectra of P2R tau (top) and 0N4R tau (bottom) bound to microtubules at the 1 : 1 molar ratio. The 2D spectra were processed using the Gaussian window function with $\text{LB} = -20$ and $\text{GB}=0.05$. The same 2D data are also shown in Fig. 1d but were processed using a sine bell window function with $\text{SSB} = 3$ to better resolve some of the peaks. (b) Overlay of selected ^{15}N cross sections, indicating some of the sequentially assigned peaks.

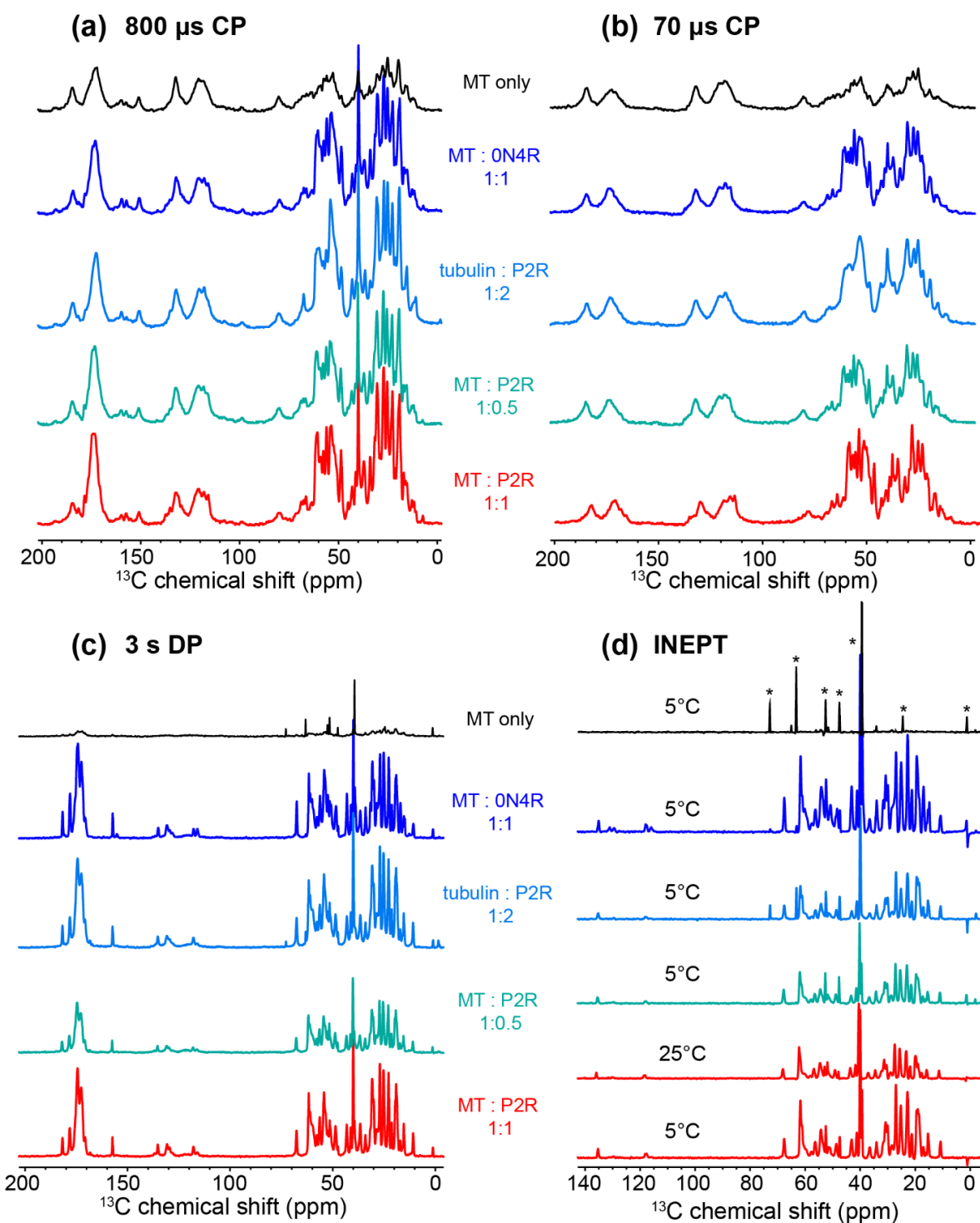


Figure S3. ^{13}C NMR spectra of microtubules with and without bound tau at varying molar ratios of microtubules and tau. Four tau-containing samples are compared: P2R tau bound to taxol-stabilized microtubules (MT) at 1 : 1 (red) and 1 : 0.5 (green) molar ratios of tubulin heterodimers to tau, tubulin co-assembled with P2R tau at 1 : 2 molar ratio (marine blue), and taxol-stabilized MTs with bound full-length 0N4R tau at 1 : 1 ratio (royal blue). The MT-only spectra (grey) are also shown for comparison. **(a)** ^{13}C CP spectra measured with 800 μs contact time, detecting semi-rigid and rigid residues. **(b)** ^{13}C CP with 70 μs contact time, detecting highly

rigid residues. **(c)** ^{13}C DP spectra measured with a 3 s recycle delay. These spectra reflect nearly quantitative intensities of all the residues. **(d)** ^{13}C INEPT spectra, detecting nearly isotropically mobile residues. Most spectra were measured on the 800 MHz NMR at $\sim 5^\circ\text{C}$. The 25°C INEPT spectrum of the 1 : 1 MT : P2R tau sample has very similar intensity patterns as the 5°C spectrum, indicating that the INEPT-detected residues are dynamic even at 5°C . Asterisks in the MT-only INEPT spectrum indicate the signals of solvents, buffer salt and small molecules such as glycerol, PIPES, DMSO, and DSS. All molar ratios refer to tubulin heterodimers to tau, and all samples contained $10\ \mu\text{M}$ taxol-stabilized microtubules (MT) or tubulin co-assembled with tau.

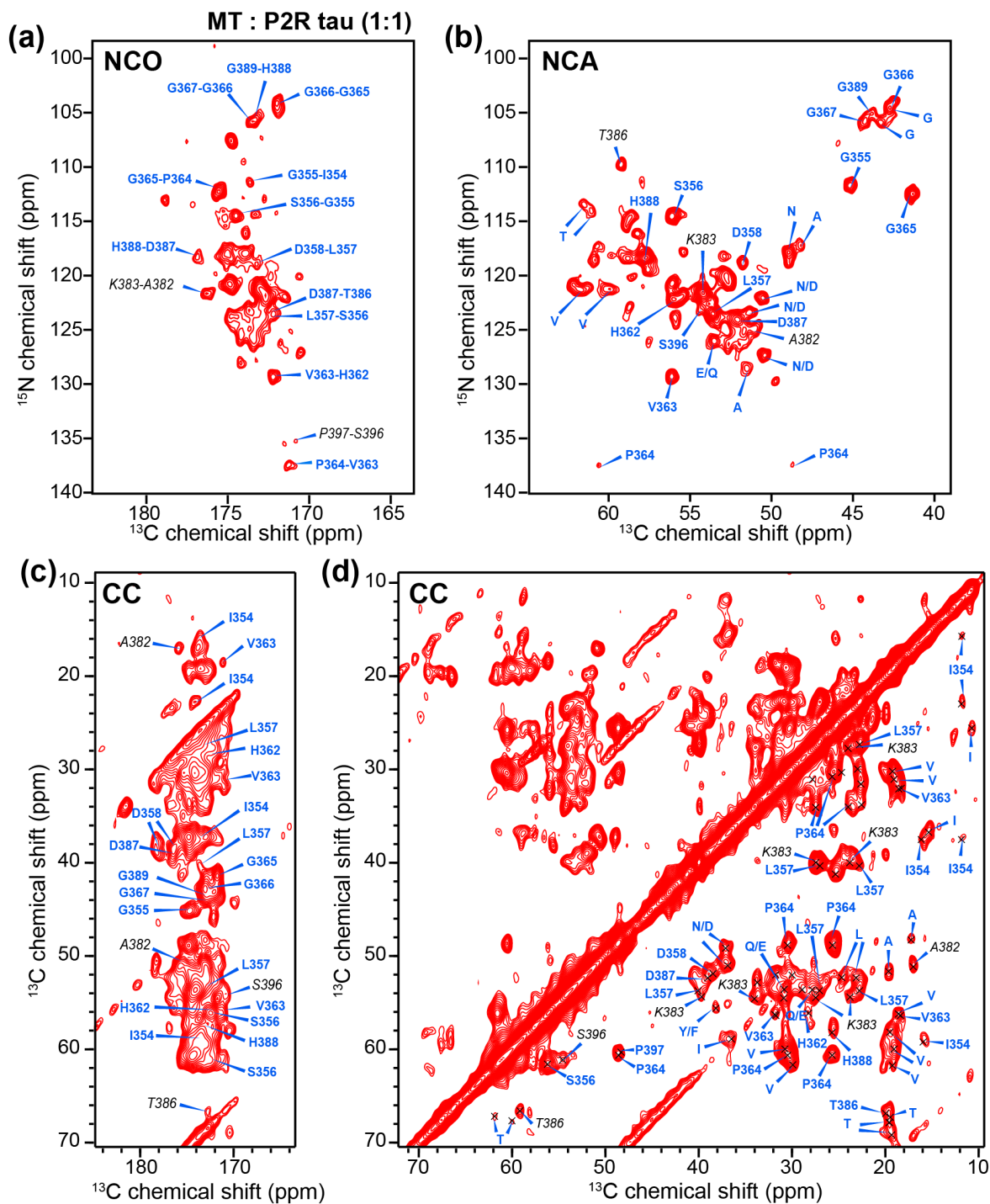


Figure S4. ^{15}N and ^{13}C chemical shifts of microtubule-bound P2R tau (1 : 1) from 2D ^{15}N - ^{13}C and ^{13}C - ^{13}C correlation spectra. Unambiguous assignments are shown in blue while ambiguous assignments are shown in black italics. (a) Inter-residue 2D NCO spectra. (b) Intra-residue 2D NCA spectrum reproduced from Figure 1d. These 2D NC spectra were processed using a sine bell window function with SSB = 2. (c) Carbonyl region of the 50 ms 2D ^{13}C - ^{13}C CORD spectrum. (d) Aliphatic region of the 50 ms 2D CC spectrum. The CC spectrum was processed using a Gaussian window function with LB = -30 and GB = 0.05 for both dimensions.

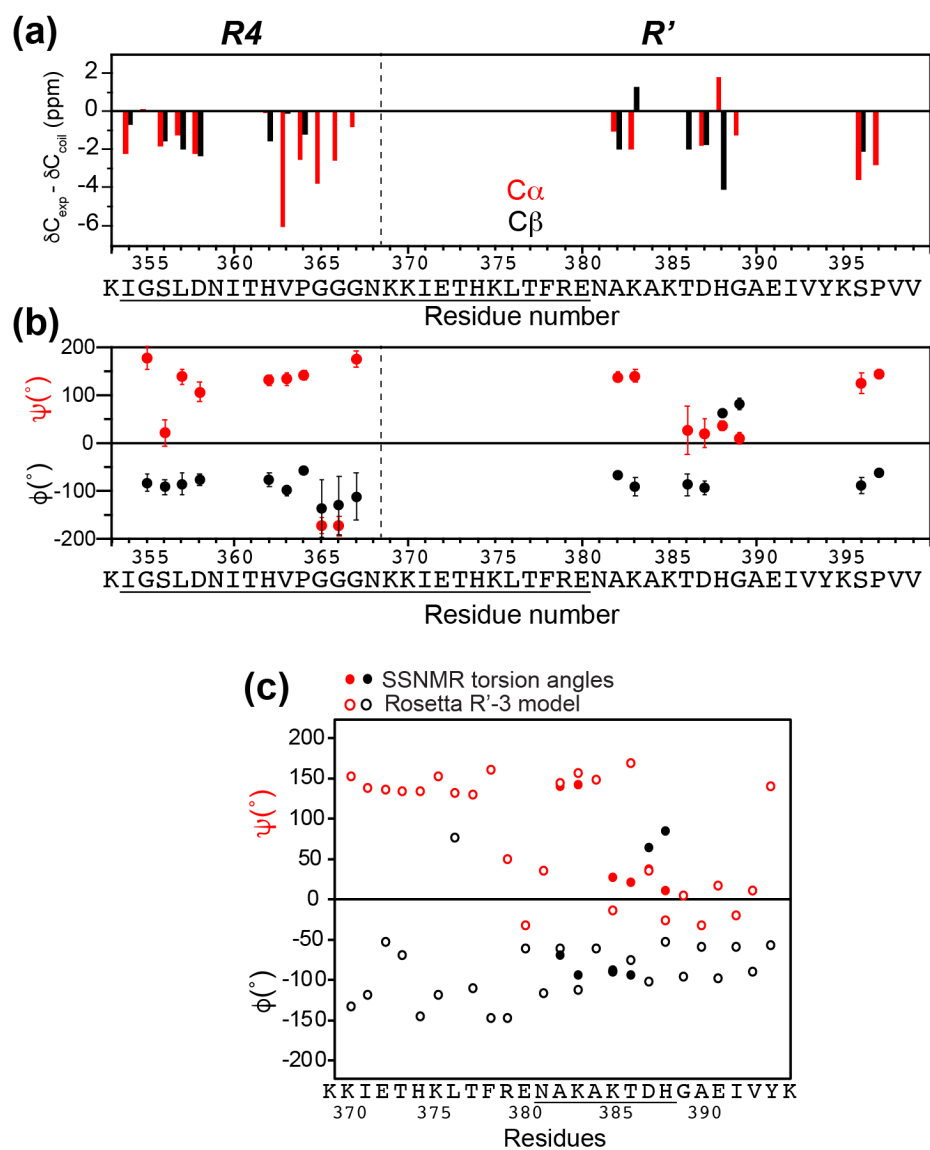


Figure S5. Backbone conformation of microtubule-bound P2R tau (1 : 1) residues. (a) $C\alpha$ and $C\beta$ secondary chemical shifts. Residues $^{353}\text{Lys-Gly}^{367}$ and $^{381}\text{Asn-Val}^{399}$ form two stretches with largely assigned chemical shifts. (b) (ϕ , ψ) torsion angles obtained from the NMR chemical shifts. (c) Comparison of the chemical-shift derived torsion angles (filled circles) with the Rosetta refined torsion angles (open circles) for $^{369}\text{Lys-Val}^{395}$ (see analysis in **Fig. S10**) The two results agree well for residues $^{381}\text{NAKAKTDH}^{388}$.

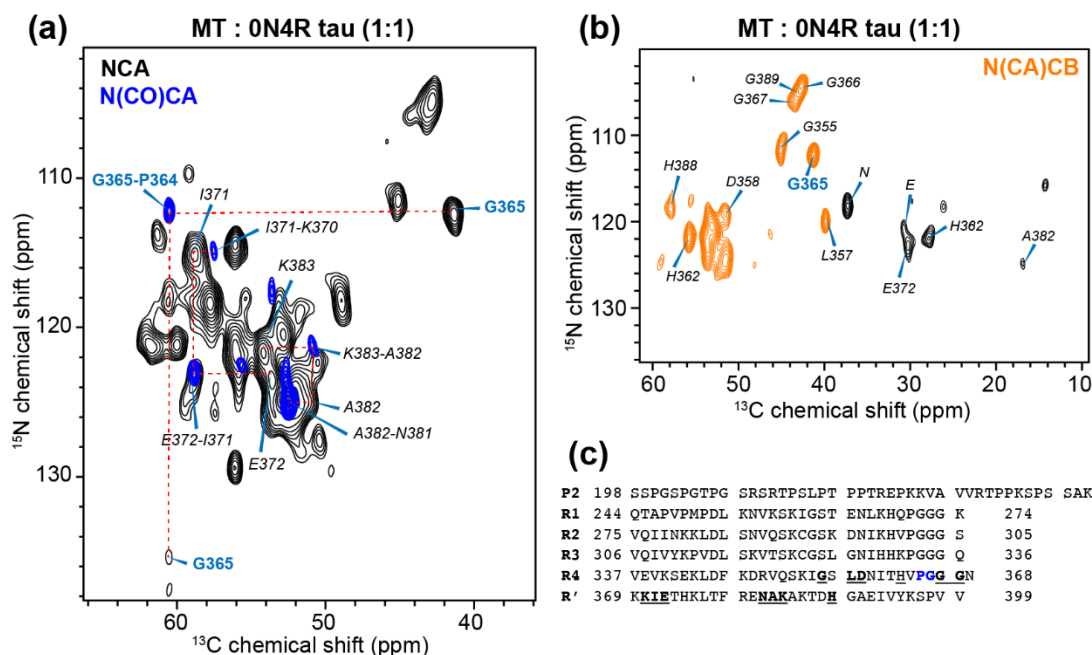


Figure S6. ^{15}N and ^{13}C chemical shift assignment of taxol-stabilized microtubule-bound 0N4R tau (1 : 1). (a) Overlay of the 2D NCA (black) and N(CO)CA (blue) spectrum. Sequential assignments are shown in blue. Ambiguous assignments are italicized and shown in black. (b) 2D N(CA)CB spectrum. Positive signals are in orange and negative $\text{C}\beta$ signals are in black. The $\text{C}\beta$ cross peaks confirm some of the sequential assignments for the MT-bound P2R tau sample (1 : 1). (c) Amino acid sequence of the five repeats of tau. Unambiguously assigned residues are shown in blue. Sequential assignments that are ambiguous or made by comparison with MT-bound P2R tau (1 : 1) are underlined.

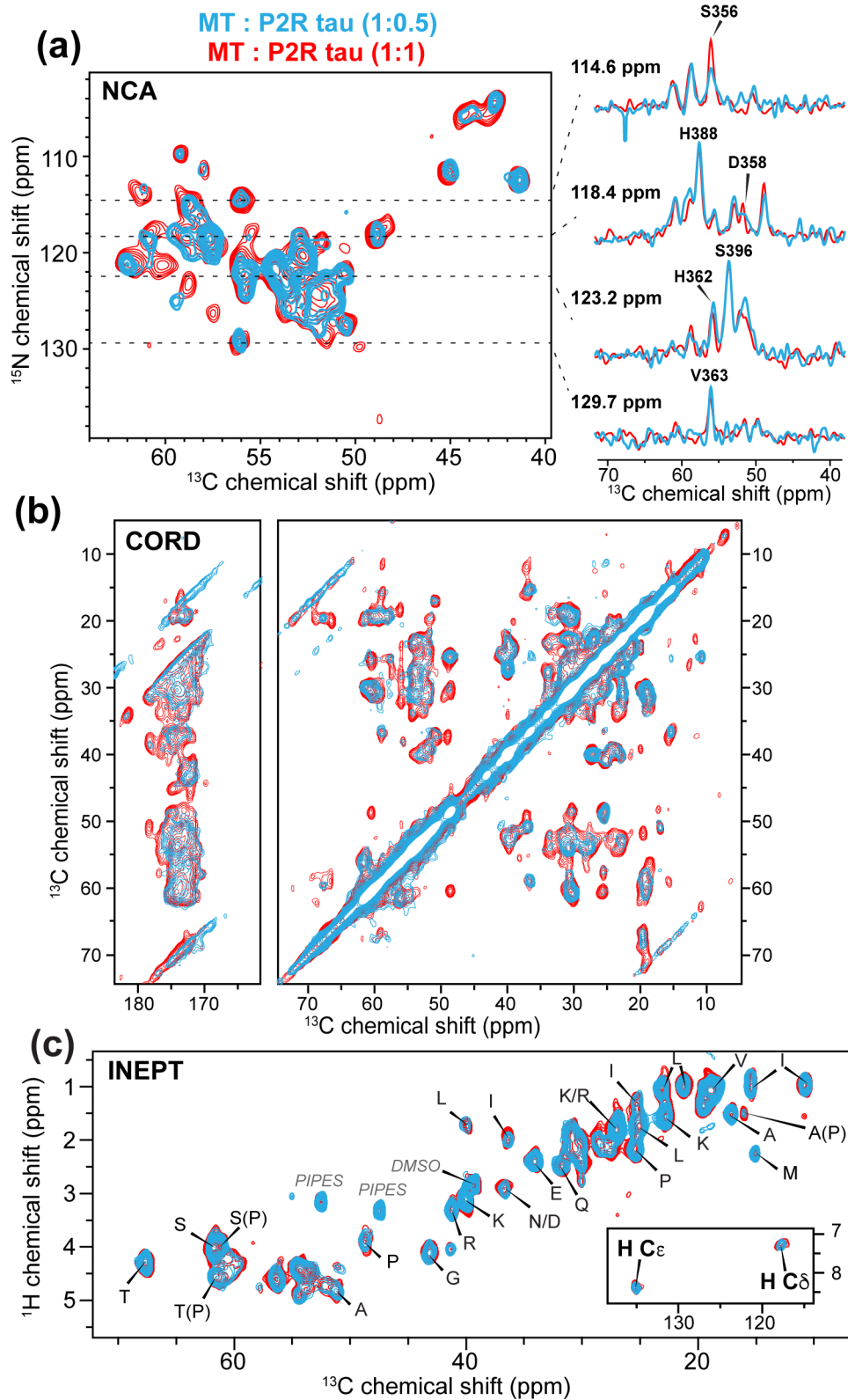


Figure S7. Taxol-stabilized microtubule-bound P2R tau adopts the same conformation at 1 : 1 and 1 : 0.5 ratios of tubulin heterodimer : tau. (a) 2D NC α spectra of the 1 : 1 (red) and 1 : 0.5 (cyan) samples and representative 1D cross sections at various ^{15}N chemical shifts. The spectral

patterns are similar between the two samples, indicating that the tau-MT interaction observed in the 1 : 1 sample is not due to crowding, and the bound domain has the same conformation at the two molar ratios. The MT concentrations were 10 μ M before packing into the MAS rotors. **(b)** 2D CC spectra of the 1 : 1 (red) and 1 : 0.5 (green) samples, measured with 50 ms ^{13}C spin diffusion at ~ 280 K under 10.5 kHz MAS. **(c)** 2D ^1H - ^{13}C INEPT spectrum of the 1 : 0.5 sample (green) compared to the 1 : 1 sample (red).

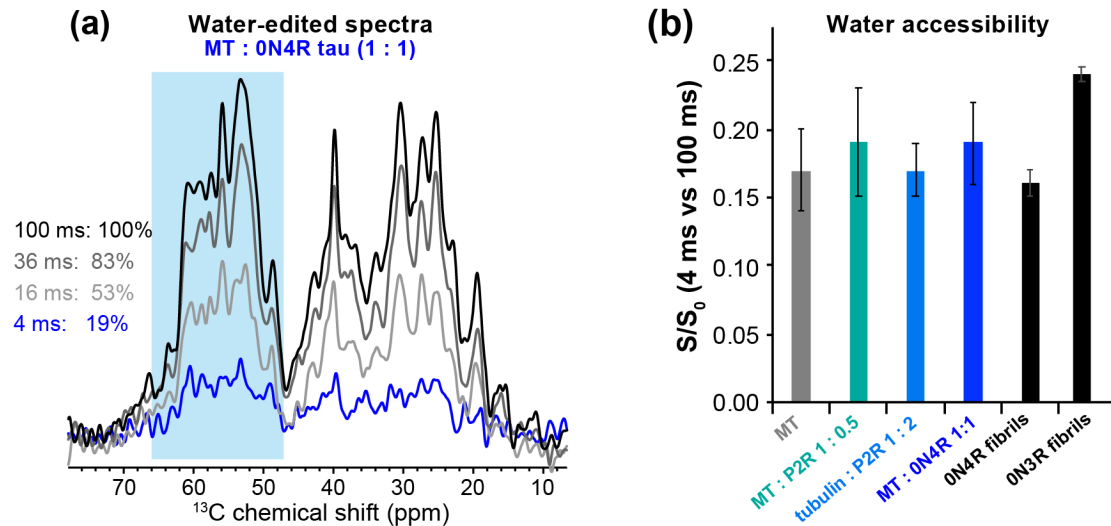


Figure S8. Microtubule-bound tau is shielded from water. (a) Water-edited ^{13}C spectra of MT-bound 0N4R tau (1 : 1), measured with ^1H spin diffusion mixing times of 4, 16, 36, and 100 ms. Intensity ratios are integrated over 46-71 ppm. (b) Water-edited intensity ratios between 4 ms and 100 ms ^1H mixing for various MT-bound tau samples compared with previously reported water-edited intensities of heparin-fibrilized 0N4R tau (19, 20) and 0N3R tau fibrils (21). The rigid domain of MT-bound tau is dehydrated: its S/S_0 value of ~ 0.19 is similar to the 0N4R and 0N3R tau fibrils' S/S_0 values of ~ 0.15 and 0.23 .

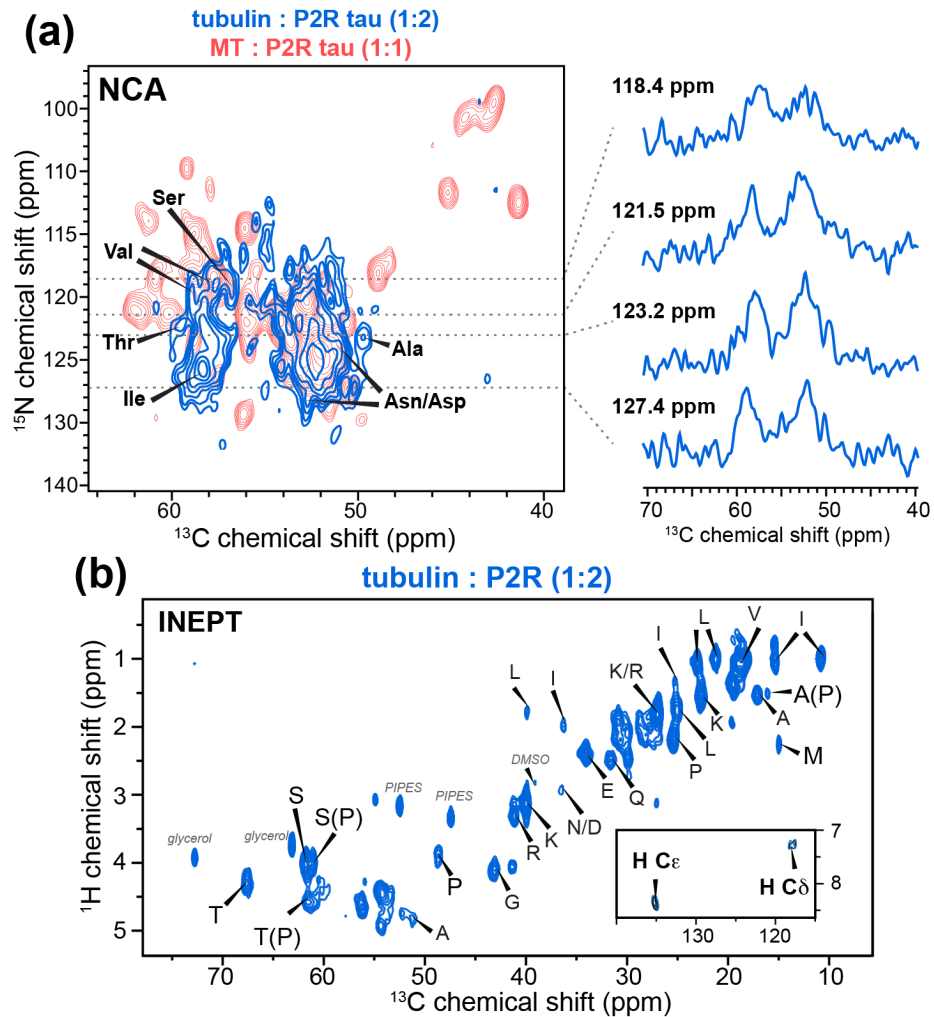


Figure S9. 2D spectra of tubulin : P2R tau (1 : 2) co-assembled sample indicate that tau binds dynamically unstable microtubules via the R' repeat. (a) 2D dipolar NCA spectrum of the tubulin : P2R tau co-assembled sample (blue, same as **Fig. 3a**) and its 1D ^{15}N cross sections. The 2D spectrum of the taxol-stabilized MT-P2R tau (1 : 1) sample is overlaid in red (same as **Fig. 1d**) for comparison. (b) 2D ^1H - ^{13}C INEPT spectrum of the tubulin – tau co-assembled sample with residue type assignment. The aromatic region of the 2D spectrum (inset) exhibits His signals but lacks Phe and Tyr signals.

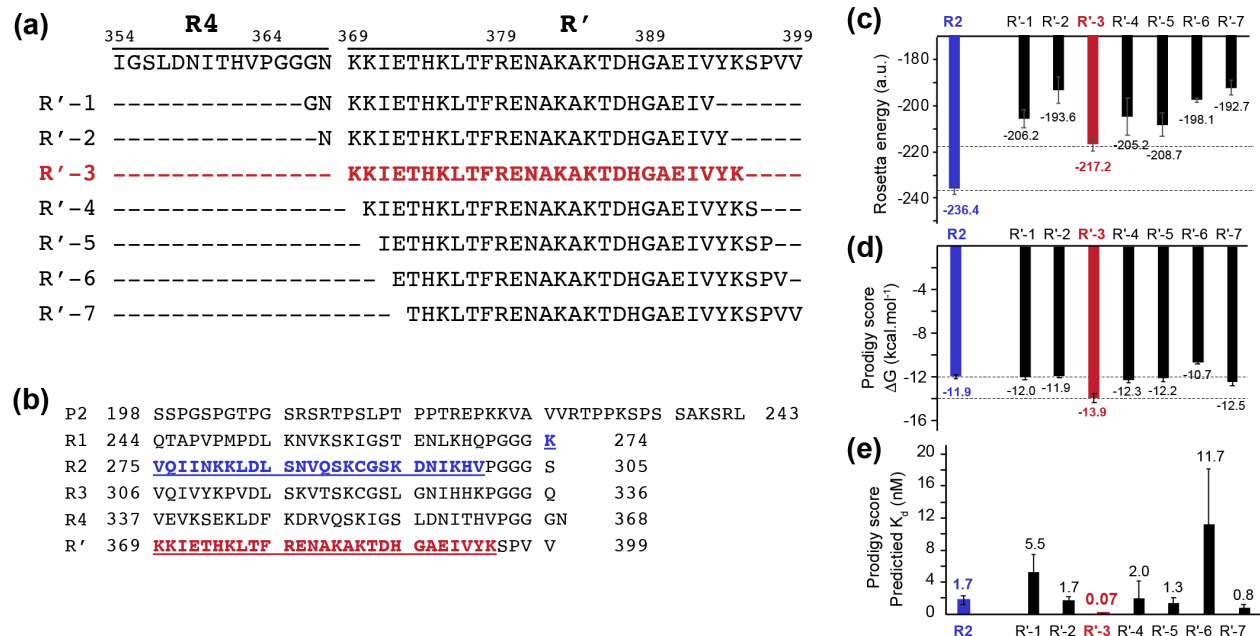
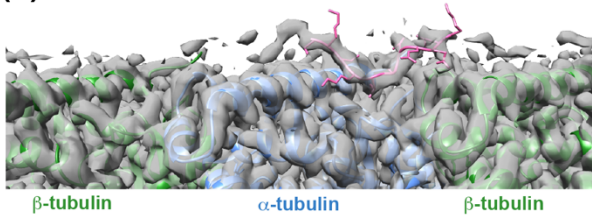
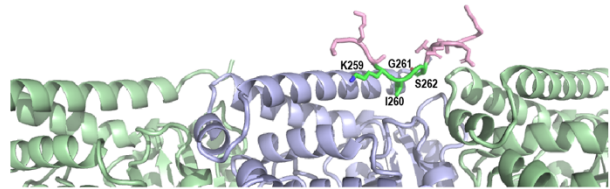


Figure S10. Structure modeling of microtubule-bound R'(369-395) using NMR chemical shifts, cryo-EM density, and Rosetta. (a) Seven 27-residue sequences in R' tested using Rosetta. The sequences are chosen based on NMR spectra showing that PGGG is excluded from the rigid domain and cryo-EM data that indicate 27 residues bound to the MT. (b) Amino acid sequence of P2R tau. R2(274-300) is shown in blue and R'(369-395) is shown in red. (c) Rosetta energy scores of the seven R' sequences against the electron densities (EMD-7771) obtained for the chimera tau construct R2 x 4. A R2(274-300) tau model (blue) was generated for comparison. Among the seven R' sequences, R'-3 gives the lowest energy. (d) Prodigy scores (26) of the 5 models with the lowest Rosetta energies for each sequence to assess binding affinities. R'-3 has the lowest ΔG (kcal.mol⁻¹) value. (e) Predicted K_d values for each 27-residue segment. R'-3 has the highest affinity (lowest K_d) to microtubules. Error bars in (c-e) are calculated based on the standard deviation of the 5 best models.

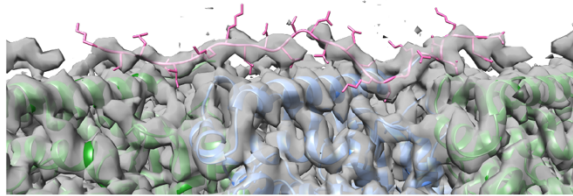
(a) EMD-7769, R1 x 4 tau (P2-R1-R1-R1-R1-R')



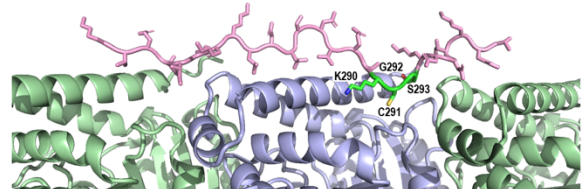
PDB: 6CVJ



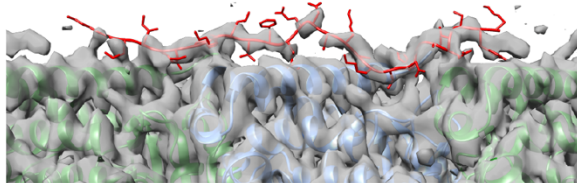
(b) EMD-7771, R2 x 4 tau (P2-R2-R2-R2-R2-R')



PDB: 6CVN



(c) EMD-7522, native tau (...P2-R1-R2-R3-R4-R'...)



R' binding model from solid-state NMR

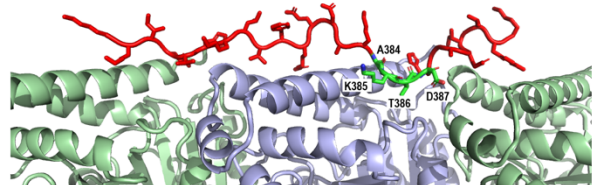


Figure S11. Structural models of the microtubule-binding domains in chimeric tau versus the microtubule-binding domain in wild-type tau. Cryo-EM density maps of three different tau constructs reported before (14) are shown on the left and the Rosetta-refined structures are shown on the right. (a) Electron density map (EMD-7769) of chimeric R1 x 4 tau best matches a 12-residue segment from V256 to K267, whose lowest energy structure model is shown on the right (pink). (b) Electron density map (EMD-7771) of chimeric R2 x 4 tau best matches a 27-residue segment from K274 to V300, whose lowest energy structure model (PDB: 6CVN) is shown on the right (pink). (c) Electron density map (EMD-7752) of wild-type tau overlaid with NMR chemical-shifts-constrained and Rosetta-refined R' lowest-energy model. This R' segment, K369 to K395, is constrained by the measured chemical shifts of the immobilized residues in the dipolar correlation solid-state NMR spectra shown here. In each of the three structural models, the four residues that show the closest approach to microtubules are indicated. These are ²⁵⁹KIGS²⁶² in R1, ²⁹⁰KCGS²⁹³ in R2, and ³⁸⁴AKTD³⁸⁷ in R'.

REFERENCES AND NOTES

1. G. M. Alushin, G. C. Lander, E. H. Kellogg, R. Zhang, D. Baker, E. Nogales, High-resolution microtubule structures reveal the structural transitions in $\alpha\beta$ -tubulin upon GTP hydrolysis. *Cell* **157**, 1117–1129 (2014).
2. M. D. Weingarten, A. H. Lockwood, S. Y. Hwo, M. W. Kirschner, A protein factor essential for microtubule assembly. *Proc. Natl. Acad. Sci. U.S.A.* **72**, 1858–1862 (1975).
3. Y. Wang, E. Mandelkow, Tau in physiology and pathology. *Nat. Rev. Neurosci.* **17**, 5–21 (2016).
4. M. Hong, V. Zhukareva, V. Vogelsberg-Ragaglia, Z. Wszolek, L. Reed, B. I. Miller, D. H. Geschwind, T. D. Bird, D. McKeel, A. Goate, J. C. Morris, K. C. Wilhelmsen, G. D. Schellenberg, J. Q. Trojanowski, V. M. Lee, Mutation-specific functional impairments in distinct tau isoforms of hereditary FTDP-17. *Science* **282**, 1914–1917 (1998).
5. G. T. Bramblett, M. Goedert, R. Jakes, S. E. Merrick, J. Q. Trojanowski, V. M. Lee, Abnormal tau phosphorylation at Ser³⁹⁶ in Alzheimer's disease recapitulates development and contributes to reduced microtubule binding. *Neuron* **10**, 1089–1099 (1993).
6. E. M. Mandelkow, E. Mandelkow, Biochemistry and cell biology of tau protein in neurofibrillary degeneration. *Cold Spring Harb. Perspect. Med.* **2**, a006247 (2012).
7. M. Goedert, R. Jakes, M. G. Spillantini, M. Hasegawa, M. J. Smith, R. A. Crowther, Assembly of microtubule-associated protein tau into Alzheimer-like filaments induced by sulphated glycosaminoglycans. *Nature* **383**, 550–553 (1996).
8. M. E. Orr, A. C. Sullivan, B. Frost, A brief overview of tauopathy: Causes, consequences, and therapeutic strategies. *Trends Pharmacol. Sci.* **38**, 637–648 (2017).
9. N. Gustke, B. Trinczek, J. Biernat, E. M. Mandelkow, E. Mandelkow, Domains of tau protein and interactions with microtubules. *Biochemistry* **33**, 9511–9522 (1994).

10. H. Kadavath, R. V. Hofele, J. Biernat, S. Kumar, K. Tepper, H. Urlaub, E. Mandelkow, M. Zweckstetter, Tau stabilizes microtubules by binding at the interface between tubulin heterodimers. *Proc. Natl. Acad. Sci. U.S.A.* **112**, 7501–7506 (2015).
11. B. Gigant, I. Landrieu, C. Fauquant, P. Barbier, I. Huvent, J. M. Wieruszeski, M. Knossow, G. Lippens, Mechanism of tau-promoted microtubule assembly as probed by NMR spectroscopy. *J. Am. Chem. Soc.* **136**, 12615–12623 (2014).
12. K. M. McKibben, E. Rhoades, Independent tubulin binding and polymerization by the proline-rich region of tau is regulated by tau's N-terminal domain. *J. Biol. Chem.* **294**, 19381–19394 (2019).
13. J. Al-Bassam, R. S. Ozer, D. Safer, S. Halpain, R. A. Milligan, MAP2 and tau bind longitudinally along the outer ridges of microtubule protofilaments. *J. Cell Biol.* **157**, 1187–1196 (2002).
14. E. H. Kellogg, N. M. A. Hejab, S. Poepsel, K. H. Downing, F. DiMaio, E. Nogales, Near-atomic model of microtubule-tau interactions. *Science* **360**, 1242–1246 (2018).
15. B. Reif, S. E. Ashbrook, L. Emsley, M. Hong, Solid-state NMR spectroscopy. *Nat. Rev. Methods Primers* **1**, 2 (2021).
16. Y. Luo, S. Xiang, P. J. Hooikaas, L. van Bezouwen, A. S. Jijumon, C. Janke, F. Forster, A. Akhmanova, M. Baldus, Direct observation of dynamic protein interactions involving human microtubules using solid-state NMR spectroscopy. *Nat. Commun.* **11**, 18 (2020).
17. S. Yan, H. Zhang, G. Hou, S. Ahmed, J. C. Williams, T. Polenova, Internal dynamics of dynactin CAP-Gly is regulated by microtubules and plus end tracking protein EB1. *J. Biol. Chem.* **290**, 1607–1622 (2015).
18. D. L. Gard, M. W. Kirschner, Microtubule assembly in cytoplasmic extracts of *Xenopus oocytes* and eggs. *J. Cell Biol.* **105**, 2191–2201 (1987).
19. A. J. Dregni, P. Duan, M. Hong, Hydration and dynamics of full-length tau amyloid fibrils investigated by solid-state nuclear magnetic resonance. *Biochemistry* **59**, 2237–2248 (2020).

20. A. J. Dregni, V. S. Mandala, H. Wu, M. R. Elkins, H. K. Wang, I. Hung, W. F. DeGrado, M. Hong, In vitro 0N4R tau fibrils contain a monomorphic β -sheet core enclosed by dynamically heterogeneous fuzzy coat segments. *Proc. Natl. Acad. Sci. U.S.A.* **116**, 16357–16366 (2019).
21. A. J. Dregni, H. K. Wang, H. Wu, P. Duan, J. Jin, W. F. DeGrado, M. Hong, Inclusion of the C-terminal domain in the β -sheet core of heparin-fibrillized three-repeat tau protein revealed by solid-state nuclear magnetic resonance spectroscopy. *J. Am. Chem. Soc.* **143**, 7839–7851 (2021).
22. S. W. Manka, C. A. Moores, Microtubule structure by cryo-EM: Snapshots of dynamic instability. *Essays Biochem.* **62**, 737–751 (2018).
23. H. Kadavath, Y. Cabrales Fontela, M. Jaremko, L. Jaremko, K. Overkamp, J. Biernat, E. Mandelkow, M. Zweckstetter, The binding mode of a tau peptide with tubulin. *Angew. Chem. Int. Ed. Engl.* **57**, 3246–3250 (2018).
24. E. Nogales, S. G. Wolf, K. H. Downing, Structure of the alpha beta tubulin dimer by electron crystallography. *Nature* **391**, 199–203 (1998).
25. S. J. Fleishman, A. Leaver-Fay, J. E. Corn, E. M. Strauch, S. D. Khare, N. Koga, J. Ashworth, P. Murphy, F. Richter, G. Lemmon, J. Meiler, D. Baker, RosettaScripts: A scripting language interface to the Rosetta macromolecular modeling suite. *PLOS ONE* **6**, e20161 (2011).
26. L. C. Xue, J. P. Rodrigues, P. L. Kastritis, A. M. Bonvin, A. Vangone, PRODIGY: A web server for predicting the binding affinity of protein-protein complexes. *Bioinformatics* **32**, 3676–3678 (2016).
27. N. Hirokawa, Y. Shiomura, S. Okabe, Tau proteins: The molecular structure and mode of binding on microtubules. *J. Cell Biol.* **107**, 1449–1459 (1988).
28. B. Niewidok, M. Igaev, F. Sundermann, D. Janning, L. Bakota, R. Brandt, Presence of a carboxy-terminal pseudorepeat and disease-like pseudohyperphosphorylation critically influence tau's interaction with microtubules in axon-like processes. *Mol. Biol. Cell* **27**, 3537–3549 (2016).
29. X. H. Li, E. Rhoades, Heterogeneous tau-tubulin complexes accelerate microtubule polymerization. *Biophys. J.* **112**, 2567–2574 (2017).

30. E. M. Mandelkow, J. Biernat, G. Drewes, N. Gustke, B. Trinczek, E. Mandelkow, Tau domains, phosphorylation, and interactions with microtubules. *Neurobiol. Aging* **16**, 355–362 (1995).
31. U. Preuss, J. Biernat, E. M. Mandelkow, E. Mandelkow, The “jaws” model of tau-microtubule interaction examined in CHO cells. *J. Cell Sci.* **110** (Pt. 6), 789–800 (1997).
32. M. D. Mukrasch, M. von Bergen, J. Biernat, D. Fischer, C. Griesinger, E. Mandelkow, M. Zweckstetter, The “jaws” of the tau-microtubule interaction. *J. Biol. Chem.* **282**, 12230–12239 (2007).
33. M. Gui, H. Farley, P. Anujan, J. R. Anderson, D. W. Maxwell, J. B. Whitchurch, J. J. Botsch, T. Qiu, S. Meleppattu, S. K. Singh, Q. Zhang, J. Thompson, J. S. Lucas, C. D. Bingle, D. P. Norris, S. Roy, A. Brown, De novo identification of mammalian ciliary motility proteins using cryo-EM. *Cell* **184**, 5791–5806.e19 (2021).
34. X. Wang, Y. Fu, W. L. Beatty, M. Ma, A. Brown, L. D. Sibley, R. Zhang, Cryo-EM structure of cortical microtubules from human parasite *Toxoplasma gondii* identifies their microtubule inner proteins. *Nat. Commun.* **12**, 3065 (2021).
35. M. R. Sawaya, S. Sambashivan, R. Nelson, M. I. Ivanova, S. A. Sievers, M. I. Apostol, M. J. Thompson, M. Balbirnie, J. J. Wiltzius, H. T. McFarlane, A. Ø. Madsen, C. Riek, D. Eisenberg, Atomic structures of amyloid cross-beta spines reveal varied steric zippers. *Nature* **447**, 453–457 (2007).
36. H. Wesseling, W. Mair, M. Kumar, C. N. Schlaffner, S. Tang, P. Beerepoot, B. Fatou, A. J. Guise, L. Cheng, S. Takeda, J. Muntel, M. S. Rotunno, S. Dujardin, P. Davies, K. S. Kosik, B. L. Miller, S. Berretta, J. C. Hedreen, L. T. Grinberg, W. W. Seeley, B. T. Hyman, H. Steen, J. A. Steen, Tau PTM profiles identify patient heterogeneity and stages of Alzheimer’s disease. *Cell* **183**, 1699–1713.e13 (2020).
37. B. Falcon, J. Zivanov, W. Zhang, A. G. Murzin, H. J. Garringer, R. Vidal, R. A. Crowther, K. L. Newell, B. Ghetti, M. Goedert, S. H. W. Scheres, Novel tau filament fold in chronic traumatic encephalopathy encloses hydrophobic molecules. *Nature* **568**, 420–423 (2019).

38. A. W. P. Fitzpatrick, B. Falcon, S. He, A. G. Murzin, G. Murshudov, H. J. Garringer, R. A. Crowther, B. Ghetti, M. Goedert, S. H. W. Scheres, Cryo-EM structures of tau filaments from Alzheimer's disease. *Nature* **547**, 185–190 (2017).
39. W. Zhang, A. Tarutani, K. L. Newell, A. G. Murzin, T. Matsubara, B. Falcon, R. Vidal, H. J. Garringer, Y. Shi, T. Ikeuchi, S. Murayama, B. Ghetti, M. Hasegawa, M. Goedert, S. H. W. Scheres, Novel tau filament fold in corticobasal degeneration. *Nature* **580**, 283–287 (2020).
40. M. Castoldi, A. V. Popov, Purification of brain tubulin through two cycles of polymerization-depolymerization in a high-molarity buffer. *Protein Expr. Purif.* **32**, 83–88 (2003).
41. A. Böckmann, C. Gardienet, R. Verel, A. Hunkeler, A. Loquet, G. Pintacuda, L. Emsley, B. H. Meier, A. Lesage, Characterization of different water pools in solid-state NMR protein samples. *J. Biomol. NMR* **45**, 319–327 (2009).
42. M. Baldus, A. T. Petkova, J. Herzfeld, R. G. Griffin, Cross polarization in the tilted frame: Assignment and spectral simplification in heteronuclear spin systems. *Mol. Phys.* **95**, 1197–1207 (1998).
43. S. A. McNeill, P. L. Gor'kov, K. Shetty, W. W. Brey, J. R. Long, A low-E magic angle spinning probe for biological solid state NMR at 750 MHz. *J. Magn. Reson.* **197**, 135–144 (2009).
44. G. Hou, S. Yan, S. Sun, Y. Han, I. J. Byeon, J. Ahn, J. Concel, A. Samoson, A. M. Gronenborn, T. Polenova, Spin diffusion driven by R-symmetry sequences: Applications to homonuclear correlation spectroscopy in MAS NMR of biological and organic solids. *J. Am. Chem. Soc.* **133**, 3943–3953 (2011).
45. J. Hoffmann, J. Ruta, C. W. Shi, K. Hendriks, V. Chevelkov, W. T. Franks, H. Oschkinat, K. Giller, S. Becker, A. Lange, Protein resonance assignment by BSH-CP-based 3D solid-state NMR experiments: A practical guide. *Magn. Reson. Chem.* **58**, 445–465 (2020).
46. S. P. Skinner, R. H. Fogh, W. Boucher, T. J. Ragan, L. G. Mureddu, G. W. Vuister, CcpNmr AnalysisAssign: A flexible platform for integrated NMR analysis. *J. Biomol. NMR* **66**, 111–124 (2016).
47. Y. Shen, A. Bax, Protein backbone and sidechain torsion angles predicted from NMR chemical shifts using artificial neural networks. *J. Biomol. NMR* **56**, 227–241 (2013).

48. J. K. Williams, M. Hong, Probing membrane protein structure using water polarization transfer solid-state NMR. *J. Magn. Reson.* **247**, 118–127 (2014).
49. T. Wang, H. Jo, W. F. DeGrado, M. Hong, Water distribution, dynamics, and interactions with Alzheimer's β -amyloid fibrils investigated by solid-state NMR. *J. Am. Chem. Soc.* **139**, 6242–6252 (2017).
50. M. G. Munowitz, R. G. Griffin, G. Bodenhausen, T. H. Huang, Two-dimensional rotational spin-echo nuclear magnetic resonance in solids: Correlation of chemical shift and dipolar interactions. *J. Am. Chem. Soc.* **103**, 2529–2533 (1981).
51. M. Hong, J. D. Gross, C. M. Rienstra, R. G. Griffin, K. K. Kumashiro, K. Schmidt-Rohr, Coupling amplification in 2D MAS NMR and its application to torsion angle determination in peptides. *J. Magn. Reson.* **129**, 85–92 (1997).
52. A. Bielecki, A. C. Kolbert, M. H. Levitt, Frequency-switched pulse sequences: Homonuclear decoupling and dilute spin NMR in solids. *Chem. Phys. Lett.* **155**, 341–346 (1989).
53. M. W. Maciejewski, A. D. Schuyler, M. R. Gryk, I. I. Moraru, P. R. Romero, E. L. Ulrich, H. R. Eghbalnia, M. Livny, F. Delaglio, J. C. Hoch, NMRbox: A resource for biomolecular NMR computation. *Biophys. J.* **112**, 1529–1534 (2017).
54. A. Vangone, A. M. Bonvin, Contacts-based prediction of binding affinity in protein-protein complexes. *eLife* **4**, e07454 (2015).
55. Y. Shi, W. Zhang, Y. Yang, A. G. Murzin, B. Falcon, A. Kotecha, M. van Beers, A. Tarutani, F. Kametani, H. J. Garringer, R. Vidal, G. I. Hallinan, T. Lashley, Y. Saito, S. Murayama, M. Yoshida, H. Tanaka, A. Kakita, T. Ikeuchi, A. C. Robinson, D. M. A. Mann, G. G. Kovacs, T. Revesz, B. Ghetti, M. Hasegawa, M. Goedert, S. H. W. Scheres, Structure-based classification of tauopathies. *Nature* **598**, 359–363 (2021).
56. Y. Wang, O. Jardetzky, Probability-based protein secondary structure identification using combined NMR chemical-shift data. *Protein Sci.* **11**, 852–861 (2002).